The Hα line emission of the Be star β Psc: the last 40 years

Ronaldo S. Levenhagen,[1]⋆ Marcos P. Diaz[2], Eduardo B. Amôres[3], and Nelson V. Leister [2]

[1]*Departamento de Física, Universidade Federal de Sao Paulo, Diadema, Brazil, Rua Prof. Artur Riedel, 275, 09972-270, Diadema, SP, Brazil*

[2] *Universidade de Sao Paulo, Instituto de Astronomia, Geofísica e Ciencias Atmosfericas, Rua do Matao, 1226 Sao Paulo, SP 05508–900, Brazil*

[3] *Departamento de Física, Universidade Estadual de Feira de Santana (UEFS), Av. Transnordestina, S/N, CEP 44036-900 Feira de Santana, BA, Brazil*

ABSTRACT

A study on the photosphere and disc of the Be star β Psc is presented. We recover almost 40 years of high-resolution spectroscopic observations and additional data gathered from the BeSS database. We evaluate the photospheric parameters from the SED and fittings of state-of-the-art non-LTE model atmospheres to observed helium, carbon, silicon and magnesium line profiles. Our models include the stellar geometric deformation as well as the co-latitude dependence of temperature and gravity, aiming to derive the effects of rotation on the stellar parameters. We estimate the circumstellar disc parameters from the fitting of models assuming different disc properties, namely its radius and gas density profile. The disc inclination angle i is constrained from the fittings of He I 4471 Å, Mg II 4481 Å, C II 4267 Å and Si II 4128, 4132 Å lines with gravity darkened models. Our findings, based on model fittings, suggest that during the last 40 years the disc radius changed within the interval $5.5 \leq R_d \leq 7.8\ R/R_*$, the disc base gas density within $5 \times 10^{-13} \leq \rho \leq 1 \times 10^{-12}$ g cm^{-3}, while the radial power-law density index m assumed values between 2.0 and 2.3. These results are in agreement with recent works dealing with spectroscopic and interferometric measurements of this object.

Key words: stars: emission-line, Be – stars: fundamental parameters – stars: circumstellar matter – radiative transfer – line: profiles – techniques: spectroscopic

1 INTRODUCTION

The emission-line B stars, assigned as Be stars, are in general main-sequence stars manifesting Balmer emission lines, sometimes associated to the occurrence of metal emission lines. Many studies today interpret these emission lines as being formed in circumstellar thin decretion discs in Keplerian motion around the central star (Rivinius et al. 2013; Rímulo et al. 2018; de Almeida et al. 2020).

Many models of the circumstellar environment, assuming different geometries, were proposed to explain the observed emission profiles and fluxes (Marlborough 1969; Huang 1972; Horne & Marsh 1986; Cidale & Ringuelet 1989; Bjorkman & Cassinelli 1993; Hummel & Vrancken 2000). The line emission varies over a broad time-scale range, which adds to conceal the dynamics of the decretion disc. Models of the disc suggest a vast parameter space even during quiescent states (Suffak et al. 2020).

In this work, we study β Psc (HR 8773, HD 217891), a bright Be star (M_V = 4.5) that we classify as a B6Ve object (Levenhagen & Leister 2004, 2006). Its Hα emission profile is bottle-shaped, and its intensity changes cyclically over the years (Abt et al. 2002; Zorec et al. 2005; Jones et al. 2011; Catanzaro 2013). Recently, Wang et al. (2018) investigated the nature and origin

of the rapid rotation of Be stars. It becomes more and more accepted that some Be stars acquired their high rotation speeds through the mechanism of mass transfer in a close binary system (Meynet 2008). In this scenario, the primary star accretes from a secondary star mass donor which end as a hot, stripped-down object. In this case, the system could be eventually identified as a Be+sdO binary. Wang et al. (2018) included β Psc in their study but they did not detect a possible hot companion through cross-correlation analysis of its UV spectra against hot stellar templates.

Previous studies reveal substantial variations in the Hα line flux with respect to the local continuum along months/years, as well as long and short-term line profile variability (Slettebak & Reynolds 1978; Andrillat & Fehrenbach 1982; Hanuschik et al. 1988, 1996; Stefl et al. 2009). However, the physical properties of the circumstellar disc of this object and their correlation with variations in the Hα profile remain unknown.

Here we present the results of the analysis of high dispersion spectroscopic (ESO/FEROS) observations and extensive synoptic data gathered from the literature. In Section 2, we present detailed information on the photometric and spectroscopic data. In Section 3 the physical parameters of the central star are estimated assuming that rapid rotation causes the flattening of the stellar poles and enlargement at the equator and as a consequence a colatitude-dependent temperature distribution (von Zeipel 1924a,b). In Section 4, we model the Hα line profiles aiming to estimate the basic parameters of the circumstellar environment for each observing epoch, namely

---

⋆ E-mail: ronaldo.levenhagen@unifesp.br (RSL)

the disc radius and gas density distribution. We discuss the results obtained in our analysis in Section 5 and the conclusion is shown in Section 6.

2   OBSERVATIONAL DATA

The photometry data handled in this work come from several sources. We exploited Johnson's 11-color photometry data by Ducati (2002)[1], 2MASS JHK_S photometry by Skrutskie et al. (2006), 13-colour photometry by Johnson & Mitchell (1975) and Gaia DR2 photometry (Gaia Collaboration et al. 2016, 2018). Also, additional photometry data by Straatman et al. (2016), Gudennavar et al. (2012), Kervella et al. (2019), Kharchenko (2001) and Morel & Magnenat (1978) were employed.

We observed the star β Psc during six nights, from 2001/Aug/02 to 2001/Oct/09 using the FEROS spectrograph (Kaufer et al. 1999) attached to the European Southern Observatory (ESO) 1.52 m telescope at La Silla (Chile). Figure 1 shows the Hα line profiles for each night of the run. Given that the Hα peak intensity and profile remained nearly constant along time-scales of several hours, we analyzed only the first spectrum of the observing night as representative of the profile's intensity for that night. Table 1 shows the leading information on these data.

It is worth noticing that even during the whole six nights, the peak intensity remained almost constant. The FEROS spectrograph sampled the optical spectrum from 3700 Å to 9000 Å, with a resolving power R= $\frac{\lambda}{\Delta\lambda} \simeq 48,000$ and a typical continuum signal-to-noise ratio of ~ 300. The simple optical setup has two fibres with 2".7 apertures, aimed to record simultaneously the incoming stellar flux and sky background. The detector is a back-illuminated CCD with 2948 X 4096 pixels, with 15 μm pixel size.

The data reduction followed standard procedures, with bias and scattered light subtraction, Echelle orders extraction, flatfielding, and wavelength calibration. We also performed the correction to the local standard of rest and continuum normalization with low-order polynomials. We conveyed data reduction with IRAF[2] package.

Besides the FEROS spectroscopic observations, we also analysed the spectroscopic data from the Be Star Spectra Database (BeSS)/ELODIE (Moultaka et al. 2004; Neiner et al. 2011) containing spectra taken in four epochs at the OHP. Observing data by several other authors in the literature were also included, as shown in Table 1 and in Figure 1. Also, a team of amateur astronomers [3] observed and provided 103 spectra in the BeSS database. We used these spectra to evaluate Hα equivalent widths and peak strengths. The BeSS database is an online catalogue that receives spectroscopic data continuously, aiming to include all known Be stars.

---

[1] https://cdsarc.unistra.fr/viz-bin/cat/II/237
[2] IRAF is a data reduction facility that was distributed by NOAO, administrated by the Association of Universities for Research in Astronomy (AURA), Inc., under a cooperative agreement with the National Science Foundation
[3] We thank Valerie Desnoux, Arnold de Bruin, André Favaro, Alun Halsey, Anton Heidemann, Christian Buil, Olivier Thizy, Michel Pujol, Carl Sawicki, Erik Bryssinck, Ernst Pollmann, Joan Guarro Fló, Jean-Noël Terry, Michel Bonnemant, Marco Leonardi, Olivier Garde, Alain Lopez, Pierre Dubreuil, Robert Buchheim, Stéphane Ubaud, Thierry Garrel, Thierry Lemoult

3   PHOTOSPHERIC PARAMETERS

We estimate the physical parameters of the stellar photosphere (T_{eff}, $\log g$, $V\sin i$) from both photometric measurements and optical spectra. Vizier2[4] (Ochsenbein et al. 2000) sourced the currently available photometric data. The fitting of observed broadband fluxes with model stellar atmospheres is useful to infer the first-order estimates of photospheric temperature and stellar radius, provided that reliable information on parallax is available.

Through our preliminary analysis by fitting a black-body, we have selected Johnson's 11-color photometry data by Ducati (2002), 2MASS JHK_S photometry by Skrutskie et al. (2006), 13-colour photometry by Johnson & Mitchell (1975) and Gaia DR2 photometry (Gaia Collaboration et al. 2016, 2018). Also, we used additional photometry data by Straatman et al. (2016), Gudennavar et al. (2012), Kervella et al. (2019), Kharchenko (2001) and Morel & Magnenat (1978). Unfortunately, most of the photometric measurements on this star come without uncertainty estimates.

Preliminary estimate of $V\sin i$ is derived from the Fourier transforms (Carroll 1933; Gray 2005) of helium line profiles in the spectra, considering the quadratic limb-darkening coefficients by Wade & Rucinski (1985).

After this preliminary estimate of the physical state of the photosphere, described mainly by its effective temperature T_{eff}, a more detailed parameter set is determined from the fittings of non-LTE models to the observed SED (Figure 2, top panel) (Levenhagen & Leister 2004, 2006; Levenhagen & Künzel 2011; Levenhagen et al. 2011, 2013a,b). We synthesized non-LTE model spectra using the SYNSPEC v.51 FORTRAN code (Hubeny et al. 1994) covering the spectral range 3000 Å to 18000 Å from plane-parallel, non-LTE atmosphere models computed with TLUSTY v.205 (Hubeny 1988). We used the wrapper SYNPLOT/IDL GUI (Hubeny, priv. comm.) to perform the whole synthesis procedure. Solar abundances from Grevesse & Sauval (1998) were considered for both atmosphere structure and spectral synthesis.

The synthetic fluxes were reddened assuming the A2 model published by Amôres & Lépine (2007) considering the star's direction, yielding E(B-V) = 0.033. This value is an agreement with those 0.031 and 0.027 obtained by Green et al. (2018) and Drimmel et al. (2003) as well as with the obtained one by Capitanio et al. (2017), e.g., E(B-V) = 0.026 ± 0.014.

Using the Cardelli et al. (1989) extinction curve, we applied the correction factor for all photometric bands from *U* to *K*. The maximum reddening correction along the analyzed SED is 16% at 3600Å being 9.5% at 5500Å.

When comparing to spherical SED models, the SED was also corrected for the effects of stellar geometrical deformation induced by rotation, hereafter geometrical flattening (GF). The main effect of rotation in a pole-on Be star is to increase the stellar brightening up to perhaps a half of magnitude (Townsend et al. 2004). In this work we inferred the correction assuming a bilinear interpolation of Mv × (B-V) data (Townsend et al. 2004), which makes the star to increase its brightening by about 0.38 mag when compared to a spherical photosphere.

The flux fittings resulted in a parallax of 7.5 ± 0.5 m.a.s. that provides the best scaling factor (Figure 2). This value is consistent with the newest Gaia DR2 parallax of 7.71 ± 0.24 m.a.s. (Gaia Collaboration et al. 2016; Gaia Collaboration 2016; Luri et al. 2018; Gaia Collaboration et al. 2018). The older estimate

---

[4] https://vizier.u-strasbg.fr/viz-bin/VizieR

Table 1. Spectroscopic data handled in this work. Each spectra is assigned to a reference code that is used in Figure 1. Amateur's data, also distributed in the BeSS database, are not included in this table.

| Date	No of spectra	MJD	Resolving power	Wavelength coverage (nm)	Instrument	Source	Reference code
2001/Aug/02	15	52124	48,000	370 - 900	FEROS/1.52m ESO La Silla	this work	FE2001-1
2001/Aug/05	23	52127	48,000	370 - 900	FEROS/1.52m ESO La Silla	this work	FE2001-2
2001/Aug/06	15	52128	48,000	370 - 900	FEROS/1.52m ESO La Silla	this work	FE2001-3
2001/Oct/07	12	52190	48,000	370 - 900	FEROS/1.52m ESO La Silla	this work	FE2001-4
2001/Oct/08	15	52191	48,000	370 - 900	FEROS/1.52m ESO La Silla	this work	FE2001-5
2001/Oct/09	19	52192	48,000	370 - 900	FEROS/1.52m ESO La Silla	this work	FE2001-6
1996/Sep/02	01	50328	45,000	389 - 681	ELODIE/1.93m OHP	BeSS database	EL1996
2001/Dec/20	01	52263	45,000	389 - 681	ELODIE/1.93m OHP	BeSS database	EL2001
2002/Nov/30	01	52608	45,000	389 - 681	ELODIE/1.93m OHP	BeSS database	EL2002-1
2002/Dec/02	01	52610	45,000	389 - 681	ELODIE/1.93m OHP	BeSS database	EL2002-2
1975/Dec/05	01	42751	2,200	655 - 657	Photoelectric scanner/72inch Lowell Obs.	Slettebak & Reynolds (1978)	SR1975
1976/Nov/05	01	43087	2,200	655 - 657	Photoelectric scanner/72inch Lowell Obs.	Slettebak & Reynolds (1978)	SR1976
1980/Dec/28	01	44601	10,000	644 - 668	Echelle/1.52m OHP	Andrillat & Fehrenbach (1982)	AF1980
1982/Aug/16	01	45197	100,000	655 - 657	Echelle/1.4m ESO La Silla	Hanuschik et al. (1988)	HA1982-1
1982/Aug/30	01	45211	100,000	653 - 659	Echelle/1.4m ESO La Silla	Hanuschik et al. (1988)	HA1982-2
1989/Jan/06	01	47532	50,000	655 - 657	Echelle/1.4m ESO La Silla	Hanuschik et al. (1996)	HA1989-1
1989/Sep/26	01	47795	50,000	655 - 657	Echelle/1.4m ESO La Silla	Hanuschik et al. (1996)	HA1989-2
1993/Sep/09	01	49239	50,000	655 - 657	Echelle/1.4m ESO La Silla	Hanuschik et al. (1996)	HA1993
1998/Nov/27	01	51144	13,000	655 - 658	FLAGS/Mount Abu IR Observatory	Banerjee et al. (2000)	BA1998
2004/Jul/30	01	53216	20,000	345 - 862	HEROS/2.0m Ondřejov	Saad et al. (2006)	SA2004
2007/Dec/18	01	54452	10,000	653 - 660	Fiber-fed Echelle/42inch Lowell Obs.	Silaj et al. (2010)	SI2007
2008/Jul/31	01	54678	21,000	430 - 680	FRESCO/91cm INAF-Catania	Catanzaro (2013)	CA2008-1
2008/Aug/03	01	54681	21,000	430 - 680	FRESCO/91cm INAF-Catania	Catanzaro (2013)	CA2008-2
2008/Sep/04	01	54713	21,000	430 - 680	FRESCO/91cm INAF-Catania	Catanzaro (2013)	CA2008-3
2008/Sep/05	01	54714	21,000	430 - 680	FRESCO/91cm INAF-Catania	Catanzaro (2013)	CA2008-4
2008/Oct/07	01	54746	21,000	430 - 680	FRESCO/91cm INAF-Catania	Catanzaro (2013)	CA2008-5
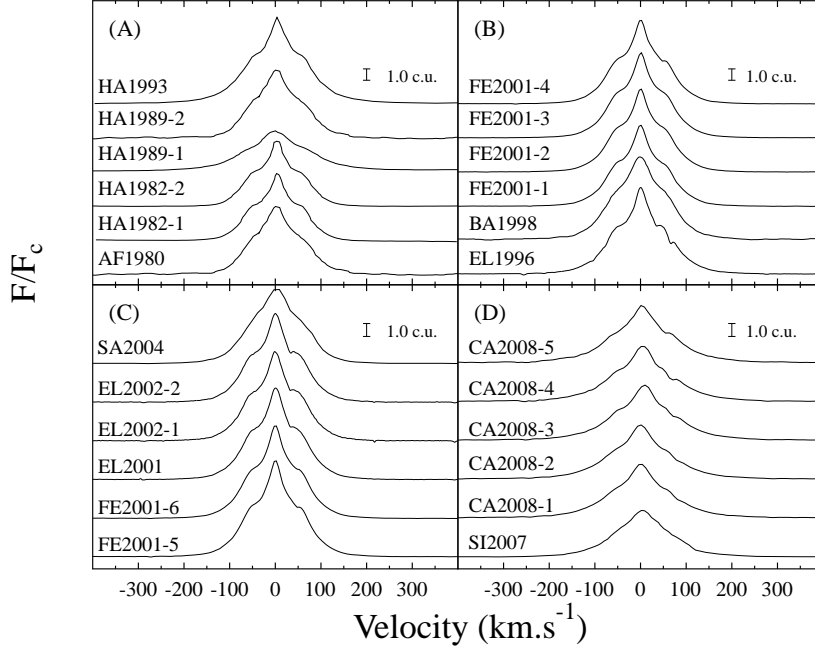
Figure 1. Hα line profiles analysed in this work. Each spectrum is assigned to a reference code shown in Table 1. The vertical bar represents the continuum unit flux.

of 6.62 ± 0.81 m.a.s. by Perryman et al. (1997) push the fittings to slightly higher T_{eff} values.

We performed the SED and spectroscopic fitting procedures with the help of a downhill simplex algorithm (Nelder & Mead 1965) in the vicinity of the starting (T_{eff}, log g, $V \sin i$) values.

The goodness of fit was evaluated using the figure-of-merit criterion (FOM) by Balian & Eddy (1977):

$$\text{FOM} = \frac{\sum_i |\Phi_{exp} - \Phi_{fit}|}{\sum_i \Phi_{fit}} \qquad (1)$$

where Φ_{exp} corresponds to the experimental data and Φ_{fit} to the fit. The FOM criterion improves on the uncertainty and fluctuations of the χ^2 formula (Balian & Eddy 1977). A FOM value lower than 2.5% points out a good fit irrespective of variations in line profile shapes and peak sizes (Balian & Eddy 1977).

The evolutionary tracks by Schaller et al. (1992), were interpolated to estimate the stellar mass $M/M_\odot$, the luminosity in log scale log $L/L_\odot$ and the age in log scale log τ fixing $Z = 0.02$.

The best fit solution is achieved for $T_{eff} = 14900 \pm 650$ K, log $g = 3.8 \pm 0.1$ c.g.s. units and parallax $\pi = 7.5 \pm 0.5$ m.a.s., with uncertainties following from the probability distributions built using the tabulated data. The complete set of parameters from the SED fitting, are shown in the left column of Table 2.

The high rotation velocities presented by Be stars, which lead the star to a non-spherical oblate shape (GF), also affects the observed line profiles in many ways. This rapidly rotating star has a polar radius that is significantly smaller than the equatorial one. This leads the atmosphere at the polar regions to receive more energy per unit area than near the equator (Collins 1963; Roxburgh et al. 1965).

Deep into the star, the radiative flux is governed by the temperature gradient, which is related to a pressure difference among the inner layers. As the star remains in hydrostatic equilibrium, the pressure gradient is ruled by gravity, while the emerging flux is proportional to the local gravity at photosphere, as stated by Von Zeipel's theorem.

The surface gravity is calculated throughout the star by evaluating the local gravitational potential gradient using the Roche approximation with the inclusion of an additional term for GF (Tassoul 1978). In this approach, we neglect multipole terms in the polynomial expansion that arise from non-uniform mass distribution (Collins & Harrington 1966). To build-up gravity-darkened (GD+GF) models, we employed the ZPEKTR code described in a previous work (Levenhagen 2014). The computed GD models depart from normal non-LTE model spectra. The simulations consider the star as a rigid rotator obeying a Roche mass distribution and suppose that the stellar rotation does not influence its core. The models are characterized by a set of parameters, such as the surface temperature, radius and gravity taken at the poles and equator, the stellar mass, the stellar rotation rate Ω/Ω_c, and the aspect angle i.

Since Be star discs are situated along the equatorial plane, to associate the aspect angle i with the disc inclination is a reasonable assumption. For each model, we made a computational mesh of thousands of area elements at the stellar surface. Each element has its local parameters $T(\theta)$ and log $g(\theta)$, where θ defines the local latitude, in agreement with the Von Zeipel's expression (von Zeipel 1924a,b; Lovekin et al. 2006). The local atmosphere structure and radiative transfer is again calculated in non-LTE using TLUSTY and SYNSPEC codes. The stellar spectrum is evaluated from the integration of the outgoing specific intensities coming from all visible elements in the line-of-sight. The whole set of model spectra is
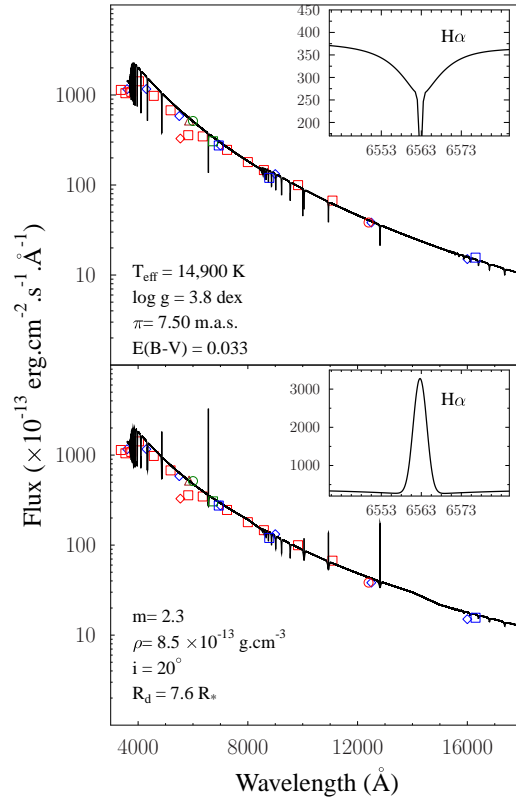

Figure 2. Top panel: Fit of synthetic non-LTE TLUSTY+SYNSPEC flux to the SED of β Psc. The model fluxes were reddened assuming the model A2 published by Amôres & Lepine (2007) with E(B-V) = 0.033. The observed SED is corrected by the brightening shift induced by geometrical distortion assuming a bilinear interpolation of Mv × (B-V) data (Townsend et al. 2004). Red squares correspond to 13-color photometry; Blue diamonds to Johnson's 11-color photometry and 2MASS; Brown triangle is assigned to Gaia DR2 photometry. Green circles stand for data from Straatman et al. (2016), red diamonds are data from Gudennavar et al. (2012), green squares are photometry by Kervella et al. (2019). Red circles are data observed by Kharchenko (2001), while blue squares are from Morel & Magnenat (1978). Top inset shows a zoomed Hα photospheric profile, with fluxes in linear scale. Bottom panel: Fit of a disc flux model plus stellar atmosphere, assuming the same extinction and geometrical distortion corrections as before. It was assumed a Keplerian velocity law for the disc (j=0.5), including shear, thermal and disc expanding velocities (see text). The fitting solution scales the gas density to $\rho = 8.5 \times 10^{-13}$ g cm^{-3}, radial index $m = 2.3$, disc radius $R_d = 7.6R_*$ and inclination angle $i = 20°$. Bottom inset shows the corresponding Hα line profile in emission. Flux is in linear scale, in the same units as the main plot.

used as a base to fit the observed spectra with the Amoeba algorithm (Nelder & Mead 1965).

Figure 3 shows the best fits of Si II $\lambda\lambda$ 4128, 4131 Å, C II λ 4267 Å, He I λ 4471 Å and Mg II λ 4481 Å profiles with gravity-darkened synthetic spectra. The basic parameters derived from these profiles are given in the right column of Table 2. For comparison purposes, we present spectra computed considering $i = 15°$ and $i = 30°$. From these fittings, it is possible to infer that the best choice for the aspect angle i is a value near $i = 20°$. As expected, the bottle-shaped, sharp Hα emission of β Psc is only compatible with a

small *i* value. The aspect angle *i* = 20° inferred from the fittings is perhaps close to its lower absolute limit, since values below *i* = 20° would lead to a break-up scenario for this star, assuming typical parameters of a main sequence B6V star. The Hα emission suggests even lower angles, although *i* = 10 − 15° would produce much deeper atmospheric profiles than those observed for most lines. These constraints on the inclination should be read with caution since they are limited by the assumption of stellar profile formation. It is difficult to precisely establish the value for *i* from the absorption profile fitting since the Mg II line appears to be filled in by the disc emission. This is possibly the case for the Si II and C II profiles as well, which may be filled in by different amounts.

4 LINE EMISSION MODELLING

We modelled the emission-line profiles with a modified version of the SHELLSPEC v.39 code (Budaj & Richards 2004), following the general outlines given in Hummel & Vrancken (2000), where the circumstellar environment is supposed to be described by an axisymmetric disc, using an exponential law for the vertical gas density distribution and a radial power-law gradient. Each gas voxel is orbiting the star at a radius *R* with Keplerian velocity given by:

$$V_{kepl} = \left(\frac{GM}{R}\right)^{1/2} \tag{2}$$

and a projected Doppler velocity shift:

$$V_D = V_{kepl} \sin i \sin \theta \tag{3}$$

where *i* stands for the aspect angle (*i* = 0 for pole-on view) and *θ* the azimuth angle concerning the line-of-sight.

Since photons originate mostly in an optically thin disc region, the Keplerian shear along the line of sight increases the Doppler gradients. We adopt the geometrical prescription for the Doppler gradient from Horne & Marsh (1986):

$$V_{shear} = -\frac{H}{2R}V_{kepl} \sin i \tan i \sin \phi \cos \phi \tag{4}$$

where *H* is the thickness of the emission layer.

We compute the Hα emission profiles by solving the line transfer equation, in LTE conditions, along the line-of-sight in the static transfer approximation. An optically thin recombination line emission prevails at the circumstellar disc medium density. The total absorption coefficient takes into account the H I bound-free opacity (Mihalas 1978; Gray 2005) and H I free-free opacity (Mihalas 1978). A pure hydrogen disc is assumed to model the Balmer lines. Thomson (Mihalas 1978) and Rayleigh (Kurucz 1970) processes contribute to the total scattering. The total emission coefficient is considered as the sum of the thermal emissivity, computed in LTE, and the scattering emissivity. The monochromatic optical depth is given by (Hummel & Vrancken 2000):

$$\tau_\nu = \frac{\pi e^2}{mc} f \rho(r,z) \frac{\lambda_0}{\sqrt{2\pi}\Delta V \cos i} \exp{-\frac{1}{2}\left(\frac{V-V_D}{\Delta V}\right)^2} \tag{5}$$

where *f* stands for the quantum oscillator strength, *ρ(r,z)* is the gas density distribution, and the resulting velocity field *ΔV* depends on the thermal broadening, the shear velocity and the disc expansion
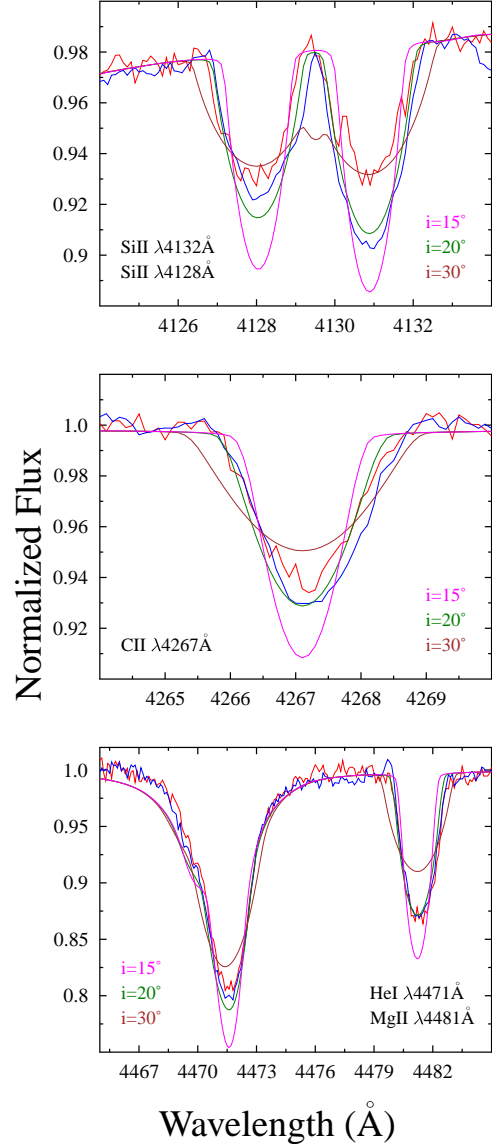

Figure 3. Fittings of FEROS (blue) and ELODIE (red) line profiles in three different regions. All non-LTE models take into account the GD and GF effects. The best fit models are obtained for Ω/Ω_c = 0.79. Top panel: Si II λλ 4128, 4131 Å line profiles in the ELODIE dataset have almost the same central depth, but in the FEROS dataset the Si II λ 4131 Å appears strengthened perhaps due to non-LTE processes in the disc. The model with *i* = 20° lies in between the others. Middle panel: both FEROS and ELODIE C II λ 4267 Å line have the same intensity and are well fitted by a model with *i* = 20°. Bottom panel: He I λ 4471 Å and Mg II λ 4481 Å line profiles are also well described with *i* = 20°. Higher *i* values (brown line, *i* = 30°) do not fit the cores while the Mg II line becomes wider than observed.

Table 2. Stellar parameters from non-LTE models to SED photometry and photospheric line profiles including GF and GD.

	SED		Line profiles
T_{eff}	14900 ± 650 K	T_{pole}	15556 ± 600 K
$\log g$	3.8 ± 0.1 c.g.s.	T_{eq}	13476 ± 600 K
$\log \tau$	7.92 ± 0.04 yr	R_p	3.60 ± 0.21 $R/R_\odot$
$\log L/L_\odot$	3.19 ± 0.26	R_e	4.09 ± 0.21 $R/R_\odot$
$M/M_\odot$	5.0 ± 0.5	$\log g_{pole}$	3.99 ± 0.14 c.g.s.
		$\log g_{eq}$	3.74 ± 0.14 c.g.s.
		$V \sin i$	90 ± 15 km s^{-1}
		Ω/Ω_c	0.79 ± 0.13
		i	$20° \pm 3°$

velocity, assuming a radial temperature profile (Stee & de Araujo 1994):

$$T_d(R) = T_{eff} (R/R_*)^\beta \tag{6}$$

We compute the emergent flux from the integration, over the solid angle, of the outcoming specific intensities from each pixel. At each pixel we evaluate the local physical variables (such as the gas density, the thermal profile, the Keplerian and expanding velocities) and after that we integrate the optical depths for each frequency point. The solution of the radiative transfer equation, reads:

$$I(\tau, \mu) = I(\tau_{layer}, \mu)e^{-\frac{(\tau_{layer}-\tau)}{\mu}} + \frac{1}{\mu} \int_\tau^{\tau_{layer}} e^{-\frac{(t-\tau)}{\mu}} S(t)dt \tag{7}$$

where $I(\tau_{layer}, \mu)$ is the incident intensity of the radiation in a layer with optical depth $\tau = \tau_{layer}$. The monochromatic flux is $F_\nu(x, y) = \int I_\nu(x, y)dxdy$ and the circumstellar material is assumed to be distributed along a thin disc with inner radius r_{in} and outer radius r_{out} with inclination angle i. The gas density $\rho(r,z)$ follows a radial power-law depending on the distance from the disc inner radius r and height from the disc midplane z (Hummel & Vrancken 2000):

$$\rho(r, z) = \rho(r_0)r^{-m} \exp\left[-\frac{1}{2}\left(\frac{z}{h(r)}\right)^2\right] \tag{8}$$

where m is the power-law index for the radial gradient, $\rho(r_0)$ is the reference gas density and $h(r)$ is the disc scale height, which is a function of the disc radius, speed of sound C_s and local disc velocity, given by (Hummel & Vrancken 2000):

$$h(r) = \frac{C_s}{V_{kepl}}R^{1.5} \tag{9}$$

where C_s follows from the mass and momentum conservation expressions and the gas state equation:

$$C_s = \sqrt{\gamma R_g T_d} \tag{10}$$

where T_d stands for the disc temperature, $R_g = 8.31434 \times 10^7$ erg.K^{-1}.mole^{-1} is the universal gas constant and $\gamma = \frac{5}{3}$ is the adiabatic expansion constant for mono-atomic gases. Through the whole fitting process, we fix the disc inclination angle i as obtained in the gravity-darkened line profile models, and vary the base gas density ρ, the power-law index m and the disc radius. Our modelling portrays a first-order approximation for the emission

line profile, providing constraints on the proposed disc parameters. A self-consistent description of the disc temperature and density structure is needed to accurately model the profiles.

5 DISCUSSION

The fitting of photometric fluxes and observed stellar spectra with non-LTE models constrain the stellar parameters to $T_{eff}= 14900 \pm 650$ K, $\log g= 3.8 \pm 0.1$ c.g.s. units and $V \sin i= 90 \pm 15$ km s^{-1}, which is compatible with a B6Ve spectral classification (Figure 2).

This result is in agreement with other studies on this object. Theodossiou & Danezis (1991) provide $T_{eff}= 15310 \pm 750$ K, while Slettebak & Reynolds (1978) and Hanuschik et al. (1996) suggest $V \sin i= 100$ km s^{-1}.

Higher T_{eff} estimates were considered by Arcos et al. (2018), who derived $T_{eff} = 16000 \pm 160$ K, $\log g= 3.00 \pm 0.03$ c.g.s. units, $V \sin i= 90 \pm 2$ km s^{-1} and assigned a B4V spectral type. Their parameters were derived by the fitting of non-LTE model spectra to He I 4471 Å and Mg II 4481 Å, with a best fit reduced χ^2 of 22.6.

Lower temperature and gravity values were reported by Frémat et al. (2005), who estimated $T_{eff}= 14359 \pm 295$ K, $\log g= 3.672 \pm 0.048$ c.g.s. units and $V \sin i= 95 \pm 5$ km s^{-1} as the apparent parameters (i.e. neglecting rotation effects) of the star, also derived by the fitting of non-LTE spectra. The different set of parameters found for this object in the literature could arise from several reasons, ranging from the accuracy of the stellar atmospheres models (e.g. number of ions, number of explicit levels, among other parameters) to the actual disc activity status. In high active phases, the disc emission can distort the line profiles and change its core depth, FWHM and wings, even for He I profiles.

Assuming rigid rotation and taking into account gravity darkening effects, the best fitting model has pole temperature $T_{pole}= 15556$ K, equator temperature $T_{eq}= 13476$ K, pole gravity $\log g_{pole}= 3.99$ and equator gravity $\log g_{eq}= 3.74$ c.g.s. units (Figure 3) with a figure-of-merit 0.64% (Balian & Eddy 1977).

This calculated FOM value shows that the observed and fitted data are in good agreement. The best-fitting model has an aspect angle $i = 20°$ and leads, for a B6 star, to a equatorial velocity $V_e = 263$ km s^{-1} assuming $V \sin i= 90$ km/s.

This value is well below the critical limit of $V_c = 416 - 418$ km/s for a B6 object (Porter 1996; Townsend et al. 2004), in agreement with Jones et al. (2008). Lower i values are reported by Catanzaro (2013) with $i = 10°$ and $V \sin i= 75$ km/s, implying a critical $V_e = 431$ km/s.

Two representative Hα line profiles and their fittings are presented in Figure 4 as an example of higher and lower emission

phases of β Psc. The spectra was normalized by the local continuum. In this figure, we display the model spectra in red. These spectra observed in 2001 and 2008 were selected for fitting our modified SHELLSPEC models assuming $1 \leq m \leq 5$, $10° \leq i \leq 50°$ and $1.0 \times 10^{-13} \leq \rho \leq 1.0 \times 10^{-11}$ g cm^{-3}. The overall line profile fittings are good, except the Hα wings that are not always well described by the model disc emission (Figure 4, lower panel). We can see significant emission in the Hα line wings well beyond the maximum expected Keplerian velocity. Such extra emission may be due to scattering of emission line photons in a low-density hot circumstellar gas.

The base gas density in the stellar disc varied within $8.8 - 6.4 \times 10^{-13}$ g cm^{-3} and the radial exponent $2.1 \leq m \leq 2.3$, adopting $i = 20°$. The external disc radius changed from $7.7R/R_*$ to $6.3R/R_*$, reflecting variations in mass loss or even viscous processes in the disc.

Besides our FEROS data, several authors observed the Hα line profiles of β Psc with different instrumentation (Slettebak & Reynolds 1978; Andrillat & Fehrenbach 1982; Hanuschik et al. 1988, 1996; Banerjee et al. 2000; Saad et al. 2006; Silaj et al. 2010) and recently, many amateur astronomers contributing to the BeSS database. The whole set of observations are not uniformly sampled in time. Over the last 40 years, one can see many gaps of months or years, which harm periodicity estimations. The Hα emission profiles always remain bottle-shaped, but their peak strengths and equivalent widths changed over the last 40 years (Figure 5). From this figure, it is possible to see only one interval with a suitable time sample to draw a disc feeding scenario, from the end of 2008 until 2010, with the shape of an ascending ramp. From that, we could probe a short time scale of a few months required to feed the disc. It is worth noticing that the equivalent widths vary between 10 and 20 Å with some correlation between equivalent widths and peak strengths, in particular during the transition to brighter line emission in 2006.

These archival data allow the investigation of basic disc parameters over a long time frame. In Figure 6, we show the range of disc radii as a function of equivalent widths for all data (top panel) and excluding the lower resolution amateur data (bottom panel). We found a good agreement between those data sets. Theoretical models with different gas densities $1.0 \times 10^{-12} \leq \rho \leq 1.0 \times 10^{-11}$ g cm^{-3} are displayed in both plots. We see that, in both plots, the whole data set fits between 5.5 and 7.8 R/R_*. Also, the data indicate a gas density region between 5×10^{-13} g cm^{-3} and 1×10^{-12} g cm^{-3}.

The gas densities found in this work are in overall agreement with the values found in the literature. A lower limit of 5.2×10^{-13} g cm^{-3} was obtained by Catanzaro (2013) while in the upper tail a value of 3×10^{-12} g cm^{-3}, with $i = 20°$ and $m = 2.3$ was found by Jones et al. (2008) and Silaj et al. (2010) using interferometric observations.

The dip seen in Figure 5, both in EW and peak height time series near MJD 54000, and in Figure 7 would suggest the occurrence of stellar brightening changes, maybe due to recent ejected material very close to the star, scattering more light to the observer. However, by inspecting the Hipparcos light curves we see that the photometry data changed only 0.03 mag during the whole mission. As the Hipparcos photometric band is large, it is mainly dominated by the continuum. So, the variability we see in peak height and EW is perhaps produced mainly by the line and not by the continuum. To mimic this stellar brightening effect, we artificially added and subtracted a factor of 0.03 mag from the continuum and re-normalized the spectra. In this case, small changes of around
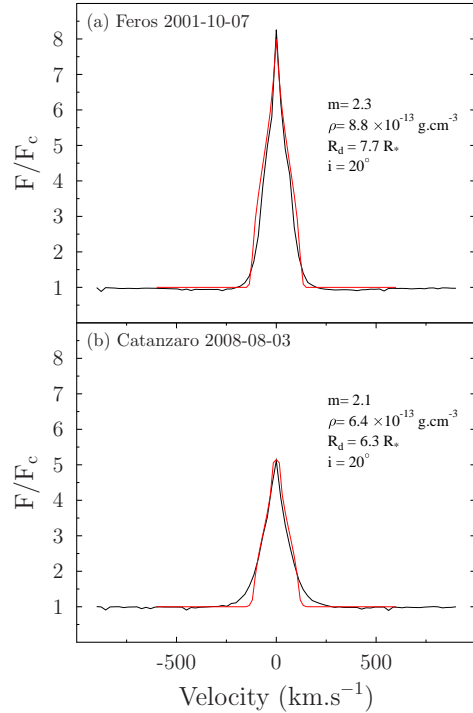
Figure 4. Model fitting of Hα line profiles with SHELLSPEC. Both models assume $i = 20°$ and isothermal gas with $T_d = 0.6T_{\rm eff}$, where $T_{\rm eff} = 14{,}900$ K. The fittings are performed over a 3-D parameter space, varying the radial exponent m, the base gas density ρ and the disc radius R_d.

1.3% in gas density and 1.2% in the stellar disc radius are obtained. Supposing, on the contrary, an upper limit case with around 0.25 mag of variation in the continuum, which is the order of magnitude seen in recent photometry by amateurs in the AAVSO database, we would have a fluctuation of about 5% in the disc radius and 12% in the gas density. Nevertheless, these data are heterogeneous and may contain non-intrinsic RMS contributions at that level. Roughly one magnitude continuum brightening would be required to produce the observed dip in the normalized line peak. However, further indication of relative continuum stability regarding the EWs and peak strengths may be found in ASAS-3 (Pojmanski et al. 2005) V-band light curve, where broadband variations below 0.2 mag on this particular time-scale are seen during the dip.

6 CONCLUSION

We present the analysis of a comprehensive Hα line profile data set of the Be star β Psc. Physical parameters of the stellar photosphere are estimated using both photometry data from the literature and fittings of line profiles with non-LTE stellar atmospheres models with geometric flattening and gravity darkening. We derive a disc inclination of $i = 20° \pm 3°$. Lower i values showed worse fittings of C II, Si II, He I 4471 Å and Mg II 4481 Å line profiles and yield equatorial velocities higher than the critical velocity.

Observing the whole Hα EW and peak strength data sets, due to the unevenly-spaced time sampling, it was not possible to find periodicities in the disc activity. However, the observed line emission variations suggest that the disc feeding occurs on timescales of a few months. Simultaneous photometric data suggests that most of large EW variations are due to the line emission.
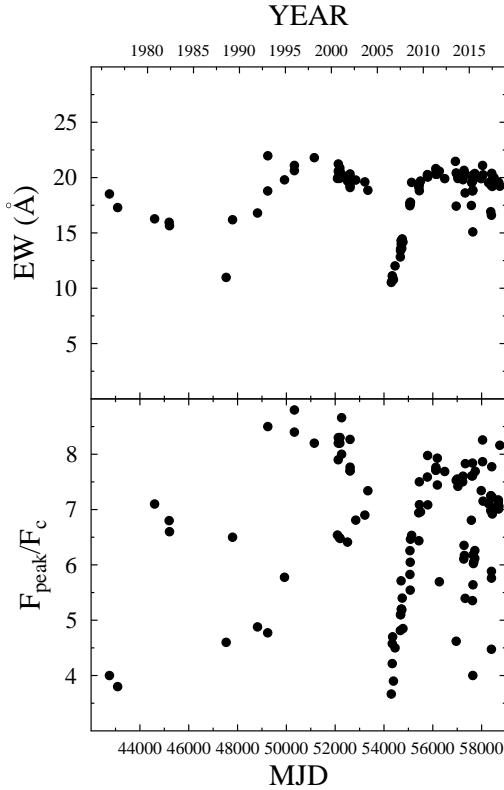
Figure 5. Top panel: Long term changes in Hα equivalent width from 1975 to 2019. The whole set of spectra is shown, including all BeSS data. Bottom panel: Hα peak strengths relative to local continuum from 1975 to 2019.

Our fittings of Hα with disc models point out that the disc changed its geometrical extent, over the last 40 years, ranging between 5.5 to 7.8 R/R_*. The mean base gas density is estimated around 7.0×10^{-13} g cm^{-3} and its radial profile is described by a power-law with index between $m = 2.0$ and $m = 2.3$. The model parameters derived from the optical spectra in this work are in reasonable agreement with the values proposed in previous works on this object (Jones et al. 2008; Catanzaro 2013).

ACKNOWLEDGEMENTS

Figure 6. Top panel: A comparison of the Hα disc radii with observed equivalent widths. All BeSS spectra (including the amateur's data) and data from literature are shown. Low panel: The same comparison, but without amateur's data. Andrillat (black open circle); Banerjee (black open square); Catanzaro (green open diamonds); Elodie (blue open triangles); Feros (red filled triangles); Hanuschik (magenta filled circles); Saad (black filled square); Silaj (black filled diamond). In all panels, the theoretical models assumed $m = 2.0$ and $i = 20°$, with the following constant gas densities: Green dashed line: model with $\rho = 5.0 \times 10^{-13}$ g cm^{-3}; Black dashed line: model with constant gas density 1.0×10^{-12} g cm^{-3}; Blue dashed line: model with 5.0×10^{-12} g cm^{-3}; Red dashed line: theoretical model with 1.0×10^{-11} g cm^{-3}.

DATA AVAILABILITY

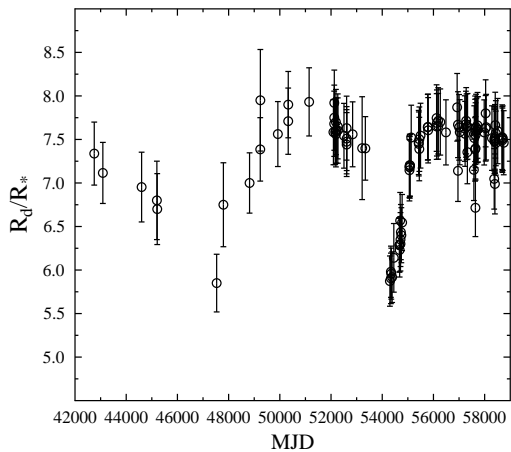The data underlying this article will be shared on reasonable request to the corresponding author.

Figure 7. Time series of the Hα disc radii. All BeSS spectra (including the amateur's data) and data from literature are shown.

Reference

Abt H. A., Levato H., Grosso M., 2002, ApJ, 573, 359
Amôres E. B., Lépine J. R. D., 2007, AJ, 133, 1519
Andrillat Y., Fehrenbach C., 1982, A&AS, 48, 93
Arcos C., Kanaan S., Chávez J., Vanzi L., Araya I., Curé M., 2018, MNRAS, 474, 5287
Balian H. G., Eddy N. W., 1977, Nuclear Instruments and Methods, 145, 389
Banerjee D. P. K., Rawat S. D., Janardhan P., 2000, A&AS, 147, 229
Bjorkman J. E., Cassinelli J. P., 1993, ApJ, 409, 429
Budaj J., Richards M. T., 2004, Contributions of the Astronomical Observatory Skalnate Pleso, 34, 167
Capitanio L., Lallement R., Vergely J. L., Elyajouri M., Monreal-Ibero A., 2017, A&A, 606, A65
Cardelli J. A., Clayton G. C., Mathis J. S., 1989, ApJ, 345, 245
Carroll J. A., 1933, MNRAS, 93, 478
Catanzaro G., 2013, A&A, 550, A79
Cidale L. S., Ringuelet A. E., 1989, PASP, 101, 417
Collins George W. I., 1963, ApJ, 138, 1134
Collins George W. I., Harrington J. P., 1966, ApJ, 146, 152
de Almeida E. S. G. d., et al., 2020, A&A, 636, A110
Drimmel R., Cabrera-Lavers A., López-Corredoira M., 2003, A&A, 409, 205
Ducati J. R., 2002, VizieR Online Data Catalog,
Frémat Y., Zorec J., Hubert A. M., Floquet M., 2005, A&A, 440, 305
Gaia Collaboration 2016, VizieR Online Data Catalog, p. I/337
Gaia Collaboration et al., 2016, A&A, 595, A2
Gaia Collaboration et al., 2018, A&A, 616, A1
Gray D. F., 2005, The Observation and Analysis of Stellar Photospheres. Cambridge University Press
Green G. M., et al., 2018, MNRAS, 478, 651
Grevesse N., Sauval A. J., 1998, Space Sci. Rev., 85, 161
Gudennavar S. B., Bubbly S. G., Preethi K., Murthy J., 2012, ApJS, 199, 8
Hanuschik R. W., Kozok J. R., Kaiser D., 1988, A&A, 189, 147
Hanuschik R. W., Hummel W., Sutorius E., Dietle O., Thimm G., 1996, A&AS, 116, 309
Horne K., Marsh T. R., 1986, MNRAS, 218, 761
Huang S.-S., 1972, ApJ, 171, 549
Hubeny I., 1988, Computer Physics Communications, 52, 103
Hubeny I., Hummer D. G., Lanz T., 1994, A&A, 282, 151

Hummel W., Vrancken M., 2000, A&A, 359, 1075
Johnson H. L., Mitchell R. I., 1975, Rev. Mex. Astron. Astrofis., 1, 299
Jones C. E., Tycner C., Sigut T. A. A., Benson J. A., Hutter D. J., 2008, ApJ, 687, 598
Jones C. E., Tycner C., Smith A. D., 2011, AJ, 141, 150
Kaufer A., Stahl O., Tubbesing S., Nørregaard P., Avila G., Francois P., Pasquini L., Pizzella A., 1999, The Messenger, 95, 8
Kervella P., Arenou F., Mignard F., Thévenin F., 2019, A&A, 623, A72
Kharchenko N. V., 2001, Kinematika i Fizika Nebesnykh Tel, 17, 409
Kurucz R. L., 1970, SAO Special Report, 309
Levenhagen R. S., 2014, ApJ, 797, 29
Levenhagen R. S., Künzel R., 2011, New Astron., 16, 307
Levenhagen R. S., Leister N. V., 2004, AJ, 127, 1176
Levenhagen R. S., Leister N. V., 2006, MNRAS, 371, 252
Levenhagen R. S., Leister N. V., Künzel R., 2011, A&A, 533, A75
Levenhagen R. S., Künzel R., Leister N. V., 2013a, New Astron., 18, 55
Levenhagen R. S., Künzel R., Leister N. V., 2013b, New Astron., 21, 27
Lovekin C. C., Deupree R. G., Short C. I., 2006, ApJ, 643, 460
Luri X., et al., 2018, A&A, 616, A9
Marlborough J. M., 1969, ApJ, 156, 135
Meynet G., 2008, in Charbonnel C., Zahn J. P., eds, EAS Publications Series Vol. 32, EAS Publications Series. pp 187–232 (arXiv:0708.3185), doi:10.1051/eas:0832006
Mihalas D., 1978, Stellar atmospheres. W H Freeman & Co.
Morel M., Magnenat P., 1978, A&AS, 34, 477
Moultaka J., Ilovaisky S. A., Prugniel P., Soubiran C., 2004, PASP, 116, 693
Neiner C., de Batz B., Cochard F., Floquet M., Mekkas A., Desnoux V., 2011, AJ, 142, 149
Nelder J. A., Mead R., 1965, Computer Journal, 7, 308
Ochsenbein F., Bauer P., Marcout J., 2000, A&AS, 143, 23
Perryman M. A. C., et al., 1997, A&A, 323, 49
Pojmanski G., Pilecki B., Szczygiel D., 2005, Acta Astron., 55, 275
Porter J. M., 1996, MNRAS, 280, L31
Rímulo L. R., et al., 2018, MNRAS, 476, 3555
Rivinius T., Carciofi A. C., Martayan C., 2013, A&ARv, 21, 69
Roxburgh I. W., Griffith J. S., Sweet P. A., 1965, Z. Astrophys., 61, 203
Saad S. M., et al., 2006, A&A, 450, 427
Schaller G., Schaerer D., Meynet G., Maeder A., 1992, A&AS, 96, 269
Silaj J., Jones C. E., Tycner C., Sigut T. A. A., Smith A. D., 2010, ApJS, 187, 228
Skrutskie M. F., et al., 2006, AJ, 131, 1163
Slettebak A., Reynolds R. C., 1978, ApJS, 38, 205
Stee P., de Araujo F. X., 1994, A&A, 292, 221
Stefl S., et al., 2009, A&A, 504, 929
Straatman C. M. S., et al., 2016, ApJ, 830, 51
Suffak M. W., Jones C. E., Tycner C., Henry G. W., Carciofi A. C., Mota B. C., Rubio A. C., 2020, ApJ, 890, 86
Tassoul J.-L., 1978, Theory of rotating stars. Princeton University Press
Theodossiou E., Danezis E., 1991, Ap&SS, 183, 91
Townsend R. H. D., Owocki S. P., Howarth I. D., 2004, MNRAS, 350, 189
von Zeipel H., 1924a, MNRAS, 84, 665
von Zeipel H., 1924b, MNRAS, 84, 684
Wade R. A., Rucinski S. M., 1985, A&AS, 60, 471
Wang L., Gies D. R., Peters G. J., 2018, ApJ, 853, 156
Zorec J., Frémat Y., Cidale L., 2005, A&A, 441, 235